JOURNAL OF MATERIALS SCIENCE 17 (1982) 1095–1102

The effect of Bi_2O_3 on the electrical and mechanical properties of ZrO_2-Y_2O_3 ceramics

K. KEIZER, A. J. BURGGRAAF
Twente University of Technology, Department of Chemical Engineering, Laboratory of Inorganic Chemistry and Materials Science, 7500 AE Enschede, The Netherlands

G. De WITH
Philips Research Laboratories, 5600 MD, Eindhoven, The Netherlands

ZrO_2–Y_2O_3 ceramics with varying Bi_2O_3 content have been prepared and their microstructure, electrical conductivity and mechanical properties investigated. The sintering rate is strongly increased at low temperatures (1270 to 1420 K) due to the occurrence of a reactive phase the amount of which decreases during the sintering process. The main fluorite phase has an approximately constant composition at 0.85 ZrO_2–0.13 Y_2O_3–0.02 Bi_2O_3 while the amount of second phase depends on overall composition and sintering procedure. The electrical conductivity is also approximately constant but about a factor of five lower than in ZrO_2–Y_2O_3 ceramics. Typical strength and fracture toughness values are 160 MPa and 1.8 MPa $m^{1/2}$, respectively. However, the non-reproducibility of the second phase content and morphology seriously influences both mechanical properties.

1. Introduction

Yttria and calcia stabilized zirconia ceramics are a well-known group of materials with a high oxygen-ion conduction at elevated temperatures. These materials are suitable for use in batteries, fuel cells, oxygen probes and sensors.

Sintering of pure stabilized zirconias is difficult because excessive grain growth occurs at temperatures of 1900 to 2000 K. This grain growth interferes with the densification process. In most cases materials with relatively low densities and microstructures consisting of large grains ($> 100\ \mu m$) and pores are obtained. These materials are not suitable for the applications mentioned.

In practice grain growth inhibitors such as SiO_2, Al_2O_3 and TiO_2 are used [1–3]. In these cases the densification occurs through a liquid phase mechanism at a relatively low sintering temperature of 1700 to 1900 K. In a preceding paper [4] the use of Bi_2O_3 powder as a sintering aid was reported for the preparation of stabilized zirconia. Relative densities near 95% and a grain size of about 5 μm could be achieved at sintering temperatures as low as 1300 to 1450 K. The high sinter-reactivity together with the low melting point and high reactivity of bismuth oxide suggests a liquid-phase mixing and sintering mechanism. The reaction of Bi_2O_3 with zirconia and yttria and the shrinkage during calcination and sintering proceeded simultaneously. With such a complex reaction mechanism it can be expected that experimental details affect the course of the reactions considerably. These experimental details are, for instance, the grain size (distribution) of the raw materials, the initial distribution of the bismuth oxide powder, the volume of the liquid phase and the amount of impurities.

Therefore in this paper some of these aspects are studied together with the effect of the final microstructures on the electrical conductivity and mechanical properties.

2. Experimental procedure

The samples were prepared as described in [4]. Prefiring and sintering conditions are given in Table I. The sample numbers in Table I are equal to the composition numbers in Fig. 1. The compositions of all samples given in Fig. 1 are deter-

0022–2461/82/041095–08$03.46/0

TABLE I Calcining and sintering data of various materials

Sample number*	Calcination		Sintering	
	T(K)	t(h)	T(K)	t(h)
1, 2	1620	16	1970	20
3, 4	1620	16	1970	65
5, 6	1320	16	1350	16
7, 11	1320	16	1350	65
8, 9†	1370	16	1420	16
10	1320	16	1350	70
12(1)†, 12(2)†	1370	16	1420 and 1570	16
13	1370	16	1420 and 1615	16
14 (citrate)	1270	1	1370	16
3 alkoxide	920	1	1370 and	3
			1670	16

*The sample number is equal to the composition number in Fig. 1.
†For Samples 9, 12(1) and 12(2), Kochlight ZrO_2 is used.

mined by X-ray fluorescence and the overall composition is given in mol%. Two other procedures were used to prepare ZrO_2–Y_2O_3 samples. Firstly, Sample 14 of ZrO_2–Y_2O_3 was prepared by the citric acid method described by Van de Graaf *et al.* [5]. After calcination Bi_2O_3 was added and this sample was sintered at 1370 K (see Table I). Secondly, the alkoxide method as described by Hoch [6] and Van de Graaf [7] was used to obtain a pure ZrO_2–Y_2O_3 ceramic (Sample 3 alkoxide) with about the same grain size and density as present in the ZrO_2–Y_2O_3–Bi_2O_3 samples.

X-ray diffraction and microstructural examination were carried out as described in [4]. The grain size was determined according to the method of Mendelsohn [8].

X-ray fluorescence spectrometry was carried out with a Philips PW1410 spectrometer to determine the overall composition of the samples [9]. Silica impurities were determined by the method reported by Kruidhof [10]. The densities were measured using the Archimedes technique.

The temperature dependence of the conductivity at 10 kHz was measured as described before [4]. Frequency dependent measurements were done in the 10 Hz to 100 kHz range with a Solartron 1174 Frequency Response Analyser on samples provided with sputtered platinum electrodes of about 0.4 μm thickness.

The fracture toughness, K_{Ic}, and strength, σ_f, were measured using the three-point bend test at a cross-head speed of 4.3 and 1.8 $\mu m\,sec^{-1}$, respectively. The sample dimensions were 1 mm by 3 mm by 15 mm and precracking was done by a Vickers hardness indentation machine (2 N load). More details are described elsewhere [11]. Both strength and fracture toughness were measured using on average eight specimens. The sample standard deviations were 15% and 5%, respectively

SEM photographs were taken from a fracture surface for each type of material, after covering the surface with a thin gold layer to eleminate charging effects.

3. Results and discussion

3.1. Materials characteristics

Various data for the samples are given in Table II. The lattice constant of the fluorite phase of the ZrO_2–Y_2O_3 samples increases slightly with increasing Y_2O_3 content, in agreement with the

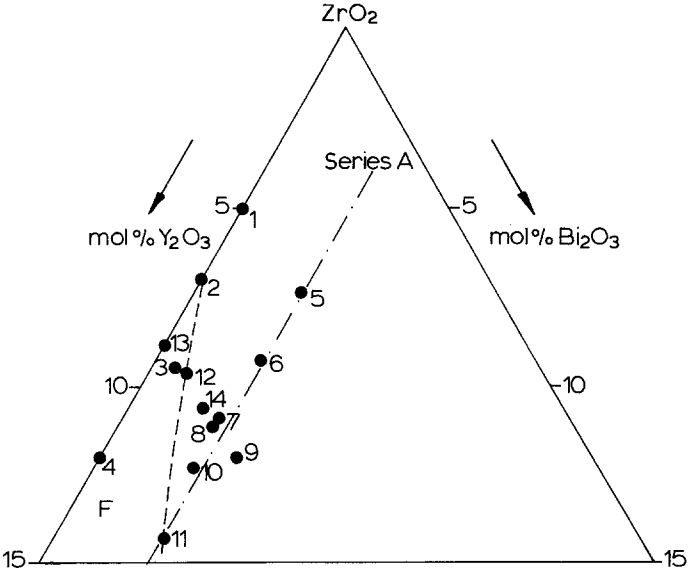

Figure 1 Compositions of the samples in the ZrO_2–Y_2O_3–Bi_2O_3 system.

TABLE II The microstructure, phases* and impurities of various ZrO_2 –Y_2O_3 –Bi_2O_3 samples

Sample number	Density† ($\times 10^{-3}$ kg m^{-3})	Average grain size (μm)	Phases*	SiO_2-content (wt%)	Sample composition (mol%)		
					ZrO_2	Y_2O_3	Bi_2O_3
1	5.91 (98.5)		F (0.5128) + M (5)	0.64	94.9	5.1	
2	5.85 (97.7)		F (0.5140)	0.62	93.1	6.9	
3	5.72 (96.1)	~ 90	F (0.5140)	0.62	91.2	8.8	
4	5.60 (94.9)	~ 90	F (0.5148)	0.60	88.0	12.0	
5	5.84 (94.5)		F (0.5153) + M (40)		92.8	4.8	2.6
6	5.85 (94.7)		F (0.5151) + M (25)		90.8	6.7	2.5
7	5.85 (95.4)	3.4	F (0.5155) + M (10)		89.2	8.5	2.3
8a	5.78 (94.1)		F (0.5157) + M (11) + U	0.62	88.9	8.8	2.3
8b	5.73 (93.3)	5.0	F (0.5152) + M (15) + U	0.62	88.8	8.9	2.3
9a	5.78 (93.6)		F (0.5158) + M (11) + U	0.14	88.0	8.7	3.3
9b	5.75 (93.2)	3.8	F (0.5155) + M (10) + U	0.14	88.0	8.7	3.3
10	5.69 (92.8)	3.2	F (0.5149) + M (< 3)		87.7	9.9	2.4
11	5.85 (95.6)	6.2	F (0.5155)		85.7	11.6	2.7
12(1)	5.66 (93.9)	15	F (0.5147)		90.3	8.8	0.9
12(2)	5.75 (94.8)	20	F (0.5146)		90.2	8.9	0.9
13	5.68 (94.2)	10–15	F (0.5145) + M (5)		90.6	8.9	0.5
14 citrate	5.65 (92.5)	4	F (0.5154) + M (3.5)	0.03	89.4	8.8	1.8
3 alkoxide	5.57 (93.5)	4	F (0.5142)	0.03	91.1	8.9	

*F is fluorite phase with the lattice parameter, a, in nm given in parentheses; the standard deviation is 0.0002 for all samples, M is monoclinic phase with the amount present in wt% given in parentheses, U is the unidentified phase.
†Figures in parenthesis are the percentage density.

literature [12, 13]. The average grain size is about 90 μm at 95 to 98% density. For the samples containing Bi_2O_3 the lattice constant of the fluorite phase is nearly constant at 0.515 nm. The grain size varies from 3 to 6 μm at 92 to 95% density.

Hence, as reported previously [4], the addition of Bi_2O_3 enables one to lower the sintering temperature several hundreds of degrees while the resulting ceramics have a comparable density and much smaller grain size.

The effect of different raw materials is demonstrated with Samples 8b/9b and 3 alkoxide/14. The microstructures of Samples 8b and 9b are presented in Figs 2 and 3. Fairly irregular microstructures containing large grains and clusters of smaller grains are observed. The composition of the large grains (fluorite phase) of Samples 8b and 9b have been analysed, with the energy dispersive X-ray analysis (EDAX) unit of the SEM, and the

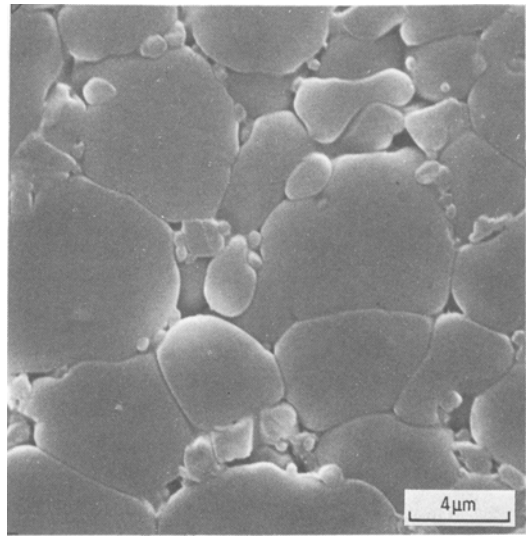

Figure 2 The ceramic microstructure of Sample 8b. (0.888 ZrO_2 –0.089 Y_2O_3 –0.023 Bi_2O_3, average grain size 5.0 μm).

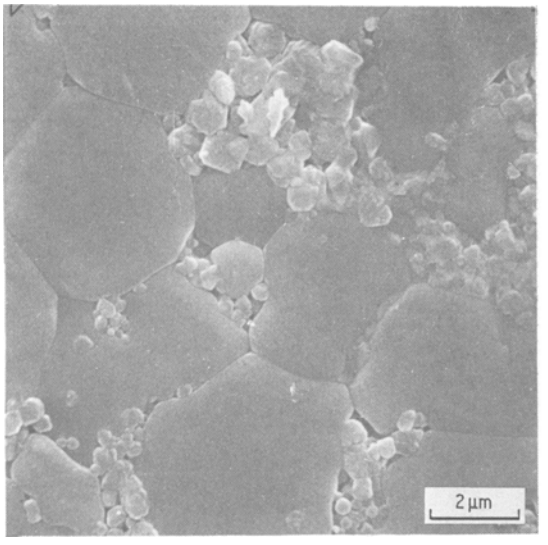

Figure 3 The ceramic microstructure of Sample 9b. (0.88 ZrO_2 –0.087 Y_2O_3 –0.033 Bi_2O_3, average grain size 3.8 µm).

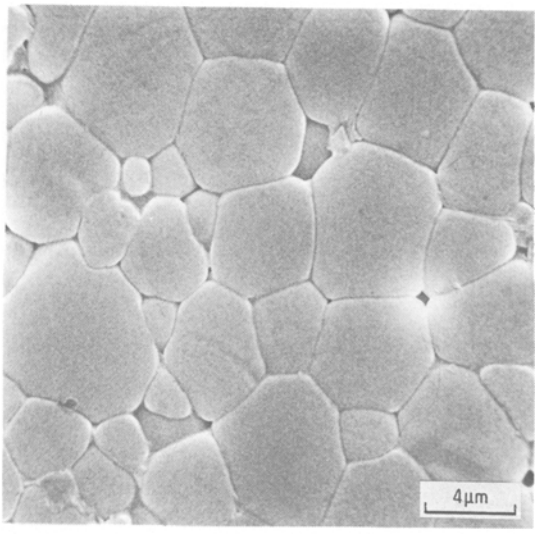

Figure 4 The ceramic microstructure of Sample 11. (0.857 ZrO_2 –0.116 Y_2O_3 –0.027 Bi_2O_3, average grain size 6.2 µm).

results are given in Table III. Analysing the smaller grains of Sample 8b (Fig. 2) the composition given in Table III is obtained. Only on the grain boundary is there a clear indication of a higher bismuth oxide content but a quantitative analysis could not be achieved. The clusters of small particles in the microstructure of Sample 9b (Fig. 3) are also analysed and the result is given in Table III. In this phase part of the Y_2O_3-material is replaced by Bi_2O_3-material compared with the overall composition of the sample. In both samples the small grain clusters contain a monoclinic (M) phase and an unidentified (U) phase. The compositions of the minor phases separately is difficult to analyse because they appear in smaller amounts and on a smaller scale. The great difference in microstructure of Samples 8b and 9b can only be ascribed to a difference in impurity content of the raw materials because the grain sizes and structure of the raw materials are about the same. The large silica content of Sample 8b, due to impurities in the zirconia raw material, can cause a low-melting, ilmenite-type $Bi_{12}SiO_{20}$ phase, which also can act as a mixing and sintering aid. An indication of this effect is, that for Sample 9b more Bi_2O_3 is necessary to obtain the same reaction and sintering effects.

TABLE III EDAX analysis of grain composition

Sample	Grain size	Composition*		
		ZrO_2	Y_2O_3	Bi_2O_3
8b	Large	0.859(15)	0.134(8)	0.008(2)
	Small	0.919(20)	0.076(10)	0.005(2)
9b	Large	0.858(13)	0.124(7)	0.016(1)
	Small	0.884(20)	0.064(8)	0.051(2)

*Figures in brackets refer to the standard deviation in the last figure(s).

The effect of different grain size of the raw materials is demonstrated with the sample pair (3 alkoxide/14) which have a grain size of 10 and 7 nm respectively. Already, at a sintering temperature of 1270 K, these powders yield ceramics with relative densities of 90 to 95% for additions of 1 to 2 mol % of Bi_2O_3.

The literature [12, 13] reports a lattice constant of 0.5154 nm for a sample of composition $0.87(1)ZrO_2$ –$0.13(1)Y_2O_3$. This value is also observed for all samples containing Bi_2O_3. This means that the introduction of a few per cent of Bi_2O_3 does not significantly affect the lattice constant and consequently the X-ray data do provide a sensitive tool for the determination of the Zr/Y ratio on the samples. This result together with the analyses of the main phases of Samples 8b and 9b leads to the conclusion that all compositions of the main, fluorite phase of the A series (Samples 5 to 11) are the same and are comparable with that of Sample 11. This sample has a composition of $0.857ZrO_2$ –$0.116Y_2O_3$ –$0.024Bi_2O_3$ and is single-phase. No indication of a second phase is present in the microstructure (Fig. 4) nor in the X-ray diffraction pattern of this ceramic.

The mechanism, resulting in a constant compo-

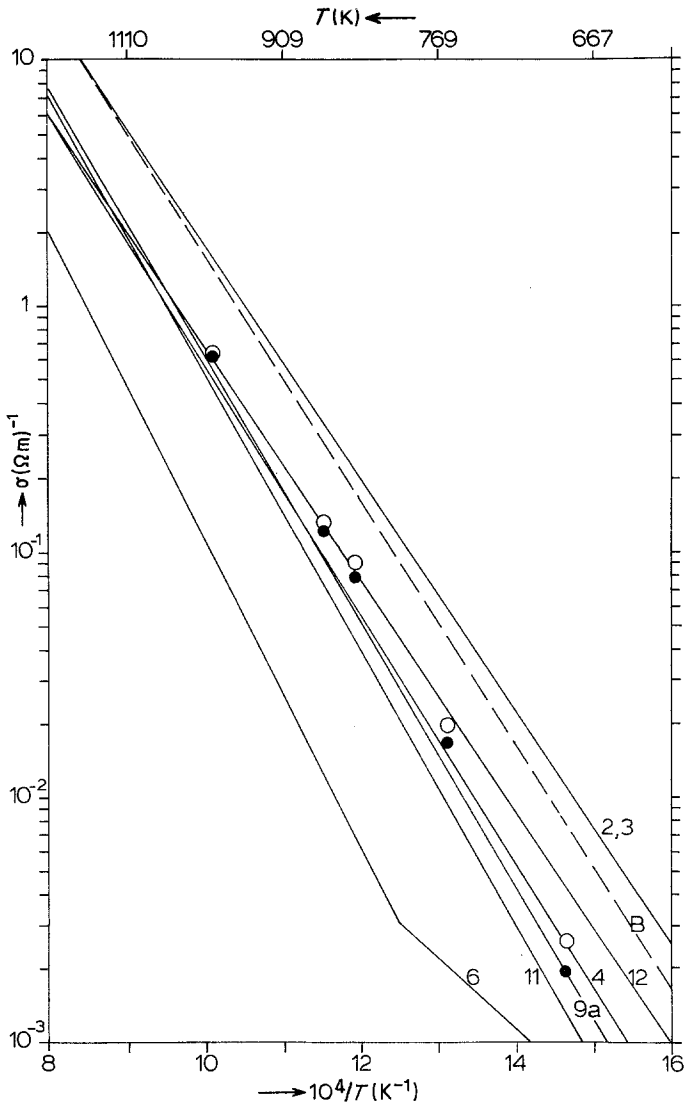

Figure 5 The electrical conductivity of various samples as a function of temperature at 10 kHz. The symbols ○ and ● denote the high and low frequency intersections respectively in the Argand diagram of Sample 9b at several temperatures.

sition of the main phase, can be explained using effects observed for the citric and alkoxide powders (Samples 14 and 3 respectively). After calcination at 1270 K and 870 K respectively the citric and the alkoxide samples were almost single-phase. After adding Bi_2O_3 to both materials and sintering at different temperature the relative Zr-rich monoclinic phase appeared, especially at the lower temperatures between 1170 K and 1370 K. Again the lattice constant of the main phase tends to the value observed for Sample 11. Together with the constant composition of the samples in Series A this suggests that Sample 11 is situated on a phase boundary of a two-phase or three-phase area. For a two-phase area the samples of Series A can be situated on or near a tie line; for a three-phase area the composition of Sample 11 may be an invariant composition in this area.

At higher temperatures Bi_2O_3-material evaporates and the monoclinic phase, which is now composed mainly of zirconia, again dissolves in the main fluorite phase. This latter effect was also observed with Samples 8b and 9b resulting in Samples 13 and 12. The microstructure of these latter materials consists of large grains with pin holes and rather irregular grain boundaries.

3.2. Conductivity of the samples

The conductivity σ of various samples is shown in Fig. 5 as a function of temperature at a constant frequency of 10 kHz. The activation energy ΔH and the σ_0-values according to the formula $\sigma =$

TABLE IV Activation energy ΔH and σ_0-values of the conductivity of various samples

Sample number	ΔH (kJ mol^{-1})	σ_0 ($\times 10^5 \Omega^{-1}$ m^{-1})
1	77	0.09
2	89	1.0
3	90	1.0
4	96	0.6
5	109	0.4
6	120	2
7	109	1.0
8b	102	1.5
9b	106	2
10	102	1.0
11	107	2
12(1)	105	1.0
13	90	0.4
B*	92	1.3

*Literature values [13, 14] of 0.91 ZrO_2 –0.09 Y_2O_3 ceramics

$\sigma_0 \exp(-\Delta H/RT)$ of these and other samples are shown in Table IV.

From Fig. 5 it can be seen that Samples 2 and 3, which contain no Bi_2O_3, have the highest conductivity at temperatures of 600 to 1200 K. The value of these conductivities is comparable with values mentioned in the literature [14] for samples with the same composition. The activation energy of the pure zirconia–yttria samples increases with increasing yttria content, which is also consistent with literature data.

The conductivity of the Bi_2O_3 containing samples is significantly lower than that of Samples 2 and 3. The conductivity of the Samples 5 and 6 is lower than for all other samples. The amount of monoclinic phase in these samples is large and probably influences the conductivity.

The activation energy of the samples of Series A is constant within a few kiloJoules at 106 kJ mol^{-1}. Furthermore, Sample 4, which contains 12 mol % Y_2O_3 and samples with 12 and 14 mol % Y_2O_3. mentioned in the literature [14] have ΔH-values of 96, 101 and 101 kJ mol^{-1}, respectively. These ΔH-values are comparable to the ΔH-value of Series A. Both facts are consistent with the idea of a main phase having a constant composition and determining the magnitude of the conductuvity of the samples

The difference in the total conductivity of Samples 5 to 11 may be ascribed to varying concentrations and kinds of impurities, to varying grain sizes and to second phases on the grain boundaries. The distinction between these different conduction mechanisms is possible using frequency dependent measurement but only for relatively simple Argand diagrams.

In Fig. 6 the Argand diagram for Sample 9b is

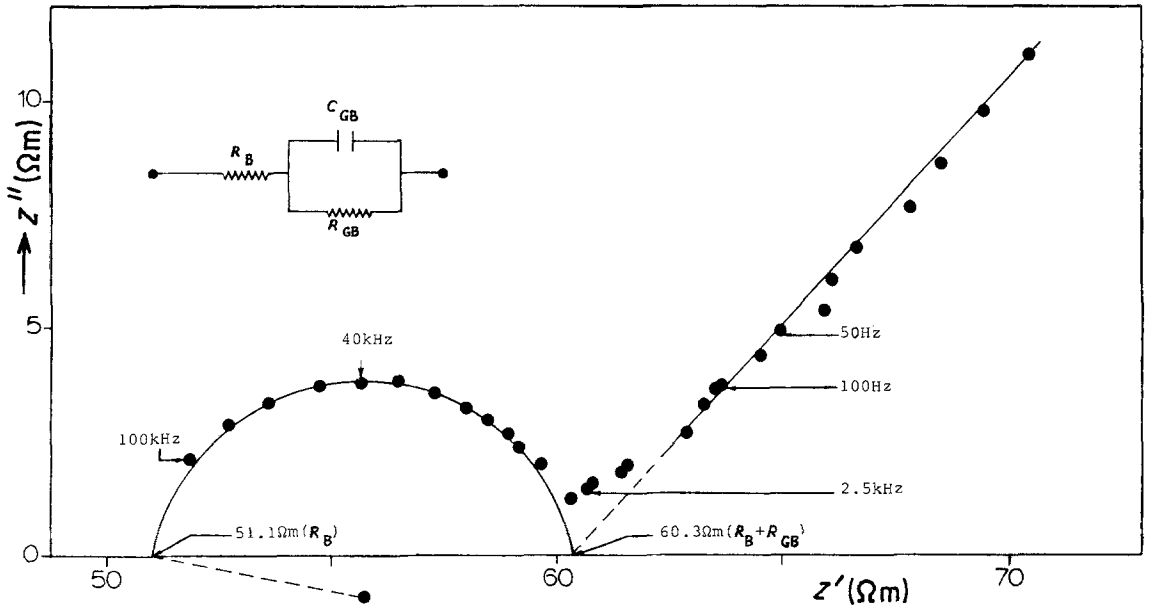

Figure 6 An Argand diagram of Sample 9b at 764 K. In the onset an electrical substitution circuit describing the frequency dispersion relation in terms of the bulk (R_B) and grain boundary resistance (R_{GB}) and grain boundary capacity (C_{GB}). Z' and Z'' denote the real and imaginary part of the impedence, respectively.

TABLE V The fracture toughness K_{Ic}, strength σ_f and Young's modulus E of several samples

Sample number	K_{Ic} (MPa m$^{1/2}$)	σ_f(MPa)	E(GPa)*
8a	2.21	254	188
8b	1.81	154	–
9a	1.57	154	185
9b	1.78	165	–
12(1)	1.70	149	–
12(2)	1.97	142	–
14	1.92	160	–
3 alkoxide	1.49	162	–

*See reference [15].

shown. The straight line between 10 Hz and 2.5 kHz can be explained by electrode effects (Warburg impedance). The semi-circle between 2.5 kHz and 100 kHz can be ascribed to grain boundary effects. A possible electrical equivalent circiut for these phenomena is also given in Fig. 6. The value of 60.3 Ωm at about 2.5 kHz is the sum of the grain boundary and the bulk resistance. The value of 51.1 Ωm at high frequencies is the bulk resistance. Both values are given in Fig. 5 for various temperatures of Sample 9b. The difference of 9.2 Ωm between both values is the total grain boundary resistance and amounts to only 20% of the bulk resistance. This type of frequency dispersion diagram is found for Samples 9b and 8b below 900 K. Above this temperature only a Warburg impedance is observed. For Samples 12 and 13 much more complicated Argand diagrams are observed.

3.3. Mechanical properties

The mechanical properties of several samples are presented in Table V. Both strength and fracture toughness values are not particularly outstanding but are more or less typical values for zirconia ceramics.

No clear trend is observed, neither for the K_{Ic} nor for the σ_f. In any case the Bi_2O_3 addition does not deteriorate either of the properties.

An annoying aspect is the variability in measured quantities from one batch to another, as shown by the sample pairs 8a, 8b and 9a, 9b. Both b samples were meant to reproduce the corresponding a samples. However this attempt was not very succesfull as can be seen from Table V. Differences of several tens of per cent are observed in the strength as well as the fracture toughness data. Examination of the fracture surfaces of both sets shows a clear difference in microstructure. Both samples with the better mechanical properties (8a, 9b) contain clusters of small grains while the other two have a more regular distribution of small grains. Samples 8a and 9b also contain the smaller amount of 2nd phase (Table I). No difference in fracture mode was observed: all Samples 8 and 9 fractured almost completely intergranularly.

It must be noted that all the ceramics except for Sample 3 alkoxide fractured almost completely along the grain boundaries, while the sample as prepared from the alkoxide process fractured completely through the grains.

4. Conclusions

The calcining and sintering rate of $ZrO_2-Y_2O_3$ ceramics is strongly increased at low temperatures for all kinds of raw materials by adding Bi_2O_3. The Bi_2O_3 reacts with the zirconia of the fluorite phase to form a reactive, perhaps even liquid, component which acts as a medium to promote the solid state reaction and shrinkage during sintering. After sintering, second phases, a monoclinic and an unidentified one, are present in amounts depending on the overall composition and the sintering temperature. For samples fired at temperature between 1270 and 1420 K the composition of the main fluorite phase is about constant at 0.85 ZrO_2 –0.13 Y_2O_3–0.02 Bi_2O_3. Therefore, the maximum conductivity of the $ZrO_2-Y_2O_3-Bi_2O_3$ sample is lower than in $ZrO_2-Y_2O_3$ materials because the optimal Zr/Y ratio for the conductivity cannot be achieved in the $ZrO_2-Y_2O_3-Bi_2O_3$ materials.

Strength as well as fracture toughness measurements yield values typical for ZrO_2 ceramics, about 160 MPa and 1.8 MPa m$^{1/2}$, respectively. A typical effect is the non-reproducibility of the second phase content and morphology. Both strength and fracture toughness are seriously influenced by this effect.

Acknowledgement

The authors are indebted to M. A. de Jongh for performing the SEM/EDAX experiments, to H. Kruidhof for performing the chemical analysis, to M. J. Verkerk for performing some experiments concerning the alkoxide preparation and to H. Hattu for carrying out the fracture experiments.

References

1. K. C. RADFORD and R. J. BRATTON, *J. Mater. Sci.* 14 (1979) 59.

2. J. F. SCHACKELFORD, P. S. NICHOLSON and W. N. SCHMELTZER, *Amer. Ceram. Bull.* **53** (1974) 86.
3. H. TAKAGI, S. KAWABORA and H. MATSUMOTO, *Sprechsaal* **107** (1974) 584.
4. K. KEIZER, M. J. VERKERK and A. J. BURGGRAAF, *Ceramurgia Int.* **5** (1979) 143.
5. M. A. C. G. VAN DE GRAAF, T, VAN DIJK, M. A. DE JONGH and A. J. BURGGRAAF, *Sci. Ceram.* 9 (1977) 75.
6. M. HOCH and K. M. NAIR, *Ceramurgia Int.* **2** (1976) 88.
7. M. A. C. G. VAN DE GRAAF, K. KEIZER and A. J. BURGGRAAF, *Sci. Ceram.* **10** (1980) 83.
8. M. I. MENDELSOHN, *J. Amer. Ceram. Soc.* **52** (1969) 443.
9. J. H. G. VAN WILLIGEN, H. KRUIDHOF and E. A. M. F. DAHMEN, *Anal. Chim. Acta* **62** (1972) 279.
10. H. KRUIDHOF, *ibid,* **99** (1978) 193.
11. G. DE WITH and N. HATTU, *J. Mater. Sci.* **16** (1981) 841.
12. W. BAUKAL and R. SCHEIDEGGER, *Ber. Dtsch. Keram. Ges.* **45** (1968) 610.
13. A. I. IOFFE, D. S. RUTMAN and S. V. KARPACHOV, *Electrochim. Acta* **23** (1978) 141.
14. R. F. W. CASSELTON, *Phys. Stat. Sol. (a)* **2** (1970) 571.
15. G. DE WITH, H. J. A. VAN DIJK and N. HATTU, *Spec. Ceram.* 7 (1980) in press.

Received 6 July
and accepted 15 September 1981